Accepted Manuscript

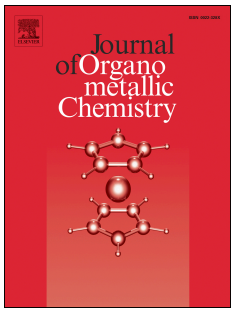

Deciphering the role of the cation in anionic cobaltabisdicarbollide clusters

Adnana Zaulet, Francesc Teixidor, Pierre Bauduin, Olivier Diat, Pipsa Hirva, Albert Ofori, Clara Viñas

PII: S0022-328X(18)30191-8

DOI: 10.1016/j.jorganchem.2018.03.023

Reference: JOM 20373

To appear in: *Journal of Organometallic Chemistry*

Received Date: 25 January 2018

Revised Date: 14 March 2018

Accepted Date: 16 March 2018

Please cite this article as: A. Zaulet, F. Teixidor, P. Bauduin, O. Diat, P. Hirva, A. Ofori, C. Viñas, Deciphering the role of the cation in anionic cobaltabisdicarbollide clusters, *Journal of Organometallic Chemistry* (2018), doi: 10.1016/j.jorganchem.2018.03.023.

Deciphering the role of the cation in anionic cobaltabisdicarbollide clusters

Adnana Zaulet,[a] Francesc Teixidor,[a] Pierre Bauduin,[b] Olivier Diat,[b] Pipsa Hirva,[c] Albert Ofori[c] and Clara Viñas[a,*]

[a] Institut de Ciència de Materials de Barcelona (ICMAB-CSIC), Campus UAB, 08193 Bellaterra, Spain.

[b.] Institut de Chimie Séparative de Marcoule, UMR 5257 (CEA-CNRS-UM-ENSCM), B.P. 17171, 30207 Bagnols sur Cèze Cedex, France.

[c] Department of Chemistry, University of Eastern Finland, Joensuu, Finland.

Dedicated to Prof. Narayan Hosmane on the occasion of his 70th birthday for his great contribution to the evolution of metallacarborane chemistry.

Abstract

The counter cation influence (H^+, Na^+, K^+ and Li^+) on the aggregates formation in aqueous solution of the salts of cobaltabisdicarbollide [**1**]$^-$ and its derivatives (monoiodinated [I-**1**]$^-$ and diiodinated [I_2-**1**]$^-$) has been studied by means of $^{11}B\{^1H\}$ and $^1H\{^{11}B\}$ NMR spectroscopy. $^{11}B\{^1H\}$ NMR spectrum of M[**1**] (M= alkali or H^+) in water exhibits much wider signals than in an organic solvent because organic solvents (acetone) cause disaggregation. The wider resonances are found at concentrations larger than 10 mM while the sharpest signals are found below 10 mM, in which a large fraction of H[**1**] is in monomeric form and only a small fraction of H[**1**] participate in the formation of vesicles that has been visualized by CryoTEM. $^{11}B\{^1H\}$ NMR of H[**1**] at concentrations lower than 10 mM corresponds to the monomer and the phase transition that is observed is due to the monomer to micelles transformation. The ^{11}B-NMR is, therefore, an excellent probe to visualize the phase transition between vesicles/monomer and micelles/monomer that appears between 10 and 20mM, for all tested cations. The $^1H\{^{11}B\}$ NMR spectra contribute interesting complementary information to the one retrieved from the $^{11}B\{^1H\}$ NMR, particularly in what concerns to dihydrogen bonds formation, C-H···H-B. These results have been compared with available crystal structures, which reveal the presence of such intermolecular dihydrogen bonds as responsible of the aggregates formation of [**1**]$^-$ in water. Computational analysis of the intermolecular interactions and self-assembly of the anions [**1**]$^-$ [I_2-**1**]$^-$ are presented.

Keywords

Metallacarborane; amphiphilic; vesicles; micelles; dihydrogen bond; cobaltabisdicarbollide.

1. Introduction

The study of carborane metal-complexes incorporating *s*-, *p*-, *d*- and *f*-block metals has attracted interest for many years.[1] The cobaltabisdicarbollide, [3,3'-Co(1,2-*closo*-$C_2B_9H_{11})_2]^-$, [**1**]$^-$, [2] is a remarkable anion: it is chemically and thermally stable in a diversity of scenarios;[3] it can be substituted at carbon or at boron atoms, [4] and regioselectively at different sites of each one of the two globes. [5] The central core of this anion, "$Co(C_2B_3)_2$", is very similar to the ferrocene core, "$Fe(C_5)_2$", thus both [**1**]$^-$ and ferrocene bear relevant resemblances, e.g. the reversible electrochemistry [6] and the high chemical and thermal stability, [3] but are different in others, such an enhanced protection of the Co in [**1**]$^-$ by a canopy of boron hydrogen units. [7] The vertexes in [**1**]$^-$ produce a rich variety of substitution sites, and are responsible for significant physicochemical properties. The first example of direct dehydrohalogenation on B in metallacarborane was done by Hawthorne et *al.* in 1967 to produce brominated species of [**1**]$^-$. [2a] Subsequently, other halogenated derivatives of [**1**]$^-$ have been reported [8], [9] and their ability to produce a stepwise modulation of the [**1**]$^-$ redox potential by each new B-X (X = halogen) unit added, studied. [10],[11]

The *in vitro* cell culture studies indicate that in [**1**]$^-$, also known as COSAN, and its mono- and diiodinated derivatives, [3,3'-Co(8-I-1,2-$C_2B_9H_{10}$)(1,2-$C_2B_9H_{11}$)]$^-$, [I-**1**]$^-$ and [3,3'-Co(8-I-1,2-$C_2B_9H_{10})_2]^-$, [I_2-**1**]$^-$, accumulate within cells. [12] Based on this knowledge, [3,3'-Co(8-I-1,2-$C_2B_9H_{10}$)(8'-R-1',2'-$C_2B_9H_{10}$)]$^-$ (R= H, $C_6H_5COO(CH_2CH_2O)_2$), respectively Na[I-**1**]$^-$ and Na[I-PEG-**1**]$^-$) compounds were radiolabeled with either ^{125}I (γ-radiation emitter) or ^{124}I (positron emitter) *via* palladium catalyzed isotopic exchange reaction, [13] and these labelled [**1**]$^-$ derivatives were administered to mice and their bio-distribution investigated by means of PET and SPECT imaging techniques. [14] These data foresee that these compounds have potential medical applications. [15] In addition, several reviews on the radioisotopes incorporation to organoboranes and boron clusters have recently appeared. [16]

Available experimental data on the behavior of [**1**]$^-$ in aqueous solution indicate clearly that its association is responsible for many of its uncommon performances, like the formation of vesicles, micelles, lamellae, [17] interaction with membranes or liposomes, [18, 12b] with aminoacids, [19] among others, and that on its turn the association capacity is due to C_c-H···H-B and other dihydrogen bonds; but we also noticed that the influence of the cation is not negligible. For example the solubility of [**1**]$^-$ salts in water, at room temperature, strongly varies according to the nature of counter cation from Na^+, Li^+, H^+, K^+ and $[NMe_4]^+$, respectively: 1509 mM, 1175 mM, 846 mM, 747 mM and 0.019 mM. [20] The Cs^+ salt was found to have the lowest solubility, 1.5 mM, of all alkaline metals. Popov et al. have found a similar series on the effect of cation on the surface pressure at the water chloro-solvent interface. [21] To learn on the former non bonding C_c-H···H-B interactions we used the weakly interacting tetramethylammonium cation.[22] In this work, we wish to extend these studies to account for the influence of the cation, and as we are more concerned to studies in solution only water soluble salts of alkaline cations (Li^+, Na^+ and K^+ including H^+) have been considered; further to learn on the influence of these cations on the widely studied halogenated derivatives of [**1**]$^-$, the highly polarizable iodinated salts of [**1**]$^-$, [3,3'-Co(8-I-1,2-$C_2B_9H_{10}$)(1,2-$C_2B_9H_{11}$)]$^-$**,** [I-**1**]$^-$ and [3,3'-Co(8-I-1,2-$C_2B_9H_{10}$)$_2$]$^-$, [I_2-1]$^-$ have been incorporated in the study.

2. Results and Discussion

2.1. Study of alkaline cations (H^+, Li^+, Na^+ and K^+) salts of [3,3'-Co(1,2-$C_2B_9H_{11}$)$_2$]$^-$, [1]$^-$, [3,3'-Co(8-I-1,2-$C_2B_9H_{10}$)(1,2-$C_2B_9H_{11}$)]$^-$, [I-**1**]$^-$ and [3,3'-Co(8-I-1,2-$C_2B_9H_{10}$)$_2$]$^-$, [I_2-**1**]$^-$.

The anionic metallacarborane [3,3'-Co(1,2-$C_2B_9H_{11}$)$_2$]$^-$, [**1**]$^-$ (Fig. 1) possess a weak coordination tendency that arises from their low charge density, [23], [4] bulky size and sufficient charge delocalization. [24] However, over the past few years, several researchers have shown that some of the metallacarboranes are not as Weakly Coordination Anions as it was thought and that they did behave similarly to a surfactant in aqueous solutions. Wipff et al. interpreted by

molecular dynamics methods that [**1**]$^-$, although lacking the amphiphilic topology, behave as anionic surfactants. [25] Later on, Matějíček et al. studied this anion in aqueous solution by a combination of static and dynamic light scattering and microscopy methods. [17b] They observed that the compound organizes in spherical aggregates with a radii of around 100 nm in a fairly monodisperse way. More recently, Bauduin et al. demonstrated by small wide-angle X-ray and neutron scattering that H[**1**] forms monolayer vesicles at low concentrations in water which radii is approx 20 nm in the concentration range 1-13 mM. [17a] Increase in concentration leads to a 1st order phase transition from vesicles to small micelles at around 13 mM. [17a] Finally, it has been proven that minor changes in the molecular structure of [**1**]$^-$ induce major modifications in the solution behavior. The substitution of two B-H by two B-I in the structure of [**1**]$^-$ to produce [I_2-**1**]$^-$ leads to a lamellae lyotropic phase at rather low concentrations, i.e. above 130 mM at ambient temperature. [17c] This minor molecular alteration, substitution of B(8)-H and B(8')-H by B(8)-I and B(8')-I, induces large self-organizing consequences that correlate very well with the concept of molecular materials.

To progress in the understanding of the solution behavior of the metallacarboranes, the performance as electrolytes of [**1**]$^-$ and its chloroderivatives, [Cl_x-**1**]$^-$ (x=2-9), in the water electrolysis process was used to ascertain if under such conditions these compounds also manifest the surfactant properties. The experiments carried out, drawn on the grounds of I/V curves of water splitting into H_2 and O_2, fully support the sentence "although lacking the amphiphilic topology, metallacarboranes behave as anionic surfactants". [26] Surfactants are amphiphilic compounds meaning that they contain hydrophobic tails and hydrophilic heads but metallacarboranes [**1**]$^-$ lack the amphiphilic topology characteristic of surfactants. [27] However, metallacarboranes at low and high aqueous concentrations display many characteristics of surfactants: self-assembly in micelles/vesicles, [17] formation of lyotropic phases, [17c] foaming [26] and surface activity [21],

[28]. Despite both clusters, [**1**]$^-$ and [I_2-**1**]$^-$, have a similar molecular structure, the type of forces that generate the aggregates are expected to be very different in the two cases.

2.2. Solid state.

To get information on the interactions between adjacent [**1**]$^-$ clusters, a search at the Cambridge Structural Database (CSD) [29] has been done, which shows 76 hits of which only 5 of them have an alkaline metal as a counteraction, four hits with Na^+ (QAJNAQ, [30] QIWTEV, [31] QOLVES [32] and XUXMOU [33]) and one with K^+ (QIWTIZ [31]). In the hits QIWTEV, QOLVES and QIWTIZ, the alkaline cation (0.95 and 1.33 Å radius for Na^+ and K^+, [34] respectively) is coordinated into the [2.2.2]cryptand cavity (approx. 1.4 Å radius) [35] acting as a super-cationic [Na[2.2.2]cryptand]$^+$ species. In the hit QAJNAQ, the Na^+ cation is six coordinate to three chelating cyclotriveratrylene (CTV) ligands. In the crystal structures QIWTEV, QOLVES and QIWTIZ, parent [**1**]$^-$ clusters have been found featuring a chain in which the metallacarborane [**1**]$^-$ clusters are bound one to the next through simple and double dihydrogen bonds B-H···H-C_c, [36] as outlined in Fig. 2. [32]

In the hit XUXMOU, [33] the crystal structure of $[Na(H_2O)_4][Co(C_2B_9H_{11})_2]$ is reported but its supramolecular structure is not studied. Fig. 3a displays that Na^+ cations form 1D chains through the axis *b*, each Na^+ cation being connected to the next one by three bridging H_2O molecules. A intermolecular dihydrogen B(8)-H(8)···H-O interaction, whose d(H···H)= 1.954Å, is observed between the [**1**]$^-$ anion an a bridging H_2O molecule of the Na^+ coordination sphere. While Fig. 3b and 3c displays that each Na^+ is surrounded by four metallacarbone clusters: two molecules interact with a short B-H···H-O contact of 1.954Å (< sum of vdW radii-0.4Å) and the other two with 2.319Å (< sum of vdW radii-0.3Å).

Hence, the presence of both B-H and C_c-H bonds in the structure is likely to be responsible for the formation of intermolecular dihydrogen bonds that produce aggregates of [**1**]$^-$ in water. Thus, the cluster C_c-H units in [**1**]$^-$ are ready to generate B-H···H-C_c dihydrogen bonds. When these

assemblies are surrounded by water molecules, they adopt a stable conformation that avoids the direct contact of the connecting non-bonding interactions with water. Therefore, in an aqueous medium, [**1**]$^-$ tend to aggregate in supramolecular entities, and similarly to the surfactants, its periphery must face water molecules. These interactions and the dimension of the aggregates prevent a facile rotation of the aggregate within the H_2O frame; the consequence is a widening of the ^{1}H NMR resonances in water. [37] Further evidence of the distinct behavior of formation of [**1**]$^-$ aggregates in water was encountered in the ^{11}B and ^{11}B{^{1}H} NMR in aqueous solution. [26] The ^{11}B NMR of H[**1**] exhibits much wider signals in water than in an organic solvent that would cause disaggregation. Consequently, all the [**1**]$^-$ are present in organic solvent as free monomers in solution.

2.3. NMR study of the H^+, Li^+, Na^+ and K^+ salts of [1]$^-$ in water.

The acid salt of cobaltabisdicarbollide H[**1**] was proven to form monolayer vesicles about 50 nm in diameter at a concentration less than 13 mM in water that was clearly observed by Cryo-TEM. [17a] However, a large increase in the hydrodynamic diameter from 50 to 890 nm was observed by dynamic light scattering (DLS) experiments after the addition of NaCl. Increasing the H[**1**] concentration over 13 mM leads to a Coulomb explosion of the closely packed monolayer vesicles into small micelles (Fig.4). The result is the coexistence of both aggregation states at concentration higher than 13 mM. The formation of monolayer vesicles and small micelles was so far unknown for water soluble carborane derivatives. [17a] It is reported that NMR is a suitable method that was well corroborated by surface tension and conductivity measurements, to determine the mechanism of aggregation. [38]

Following these studies, the Na^+, K^+ and Li^+ salts of cobaltabisdicarbollide were prepared by cation exchange as an advanced alternative to the extraction procedure in diethyl ether that leads primarily to the protonated cobaltabisdicarbollide. [39] To get the desired cation counterbalancing the cobaltabisdicarbollide, [37a] appropriately 100 mg of starting Cs[**1**] compound was dissolved in a

minimum volume of acetonitrile/water (50:50). Then, the solution of Cs[**1**] was passed repeatedly through a cation exchange resin, previously loaded with the desired cation. The solvent mixture was finally evaporated. The solubilization of the new salt in distilled water was indicative of the full cation exchange or, alternatively if $[NMe_4][\mathbf{1}]$ was the starting material, the disappearance of the $[NMe_4]^+$ peak in the ^1H NMR was diagnostic of complete exchange to the desired alkaline ion. Salts of H^+, Li^+, Na^+ and K^+ of $[\mathbf{1}]^-$ were obtained by this procedure and they were fully characterized (S.I.).

To visualize the hollow structure vesicles of the Na[**1**] salt, Cryo-TEM images of 1 mM aqueous solution of Na[**1**] were obtained and reported here for the first time. Fig. 5 displays the spherical nanovesicles of the Na[**1**] salt with a diameter about 54 nm which is very similar to the one of the H[**1**] as written above.

NMR measurements give information about the molecules in the bulk of the solution, therefore providing information on their aggregation in one particular solvent. To further evidence the behavior of the anions $[\mathbf{1}]^-$ and its monoiodinated and diiodinated derivatives, $[I\text{-}\mathbf{1}]^-$ and $[I_2\text{-}\mathbf{1}]^-$, the $^{11}B\{^1H\}$ and $^1H\{^{11}B\}$ NMR studies in D_2O of H[**1**], Li[**1**], Na[**1**], K[**1**], H[I-**1**], Na[I-**1**], H[I_2-**1**] and Na[I_2-**1**] at different concentrations (2.5, 5, 10, 20, 30, and 60 mM) were carried out.

Contrary to what is expected for common molecules by which, as a general rule, the smaller the molecule the slower the relaxation time and therefore a higher ability to record a meaningful signal, in what concerns the aqueous behavior of H[**1**], Li[**1**], Na[**1**] and K[**1**] it is observed from the $^{11}B\{^1H\}$ NMR spectra of (Fig. 6) that wider resonances are found at concentrations larger than 10 mM and that signals sharpness improve at lower concentrations. Easily observable is the fate of the peak near -21 ppm that corresponds to B(6,6') [40] and is absent or non-visible at concentrations of $[\mathbf{1}]^-$ higher than 10mM irrespective of the cation. This, in similarity with proteins´ NMR signals, [41] can be interpreted by tumbling motions of the aggregates of $[\mathbf{1}]^-$, which interfere with the alignment of nuclear spin with the external magnetic field affecting the $^{11}B\{^1H\}$ NMR

relaxation data at various concentrations of [**1**]$^-$. These data indicate that at low concentrations, the $^{11}B\{^1H\}$ NMR spectrum displays a trace with sharp signals whereas at higher concentrations, above 10 mM, when micelles are generated the signals become wider. Previous SANS investigation on the self-assembly H[**1**] in water concluded that a large (undetermined) fraction of H[**1**] is under monomeric form and only a small fraction of H[**1**] participate the formation of vesicles. Therefore H[**1**] vesicles cannot be detected by NMR as they are too large and they are present at a too low concentration. As a consequence the increase in the broadness of the NMR signal above around 10mM can be associated to the monomer to micelles. Another remarkable feature of Fig. 6 is that no noticeable differences are found between the traces of the $^{11}B\{^1H\}$ NMR of H[**1**], Li[**1**], Na[**1**] and K[**1]** that suggests that the phase transition between vesicles/monomer and micelles appears between 10 and 20mM, for all tested cations. Indeed the $^{11}B\{^1H\}$ NMR spectra show a clear change in the signals' sharpness and in the presence of the -21ppm peak at 10 and 20 mM for H[**1**], Li[**1**], Na[**1**] and K[**1].** This is in agreement with the complementary studies done with the X-ray/neutron scattering techniques [17a] and surface tension, that indicate an onset of micellization in this concentration range (10-20mM). [28] The ^{11}B-NMR is an excellent probe then, complementary to the others described to run aqueous experiments because of its short relaxation time (due to ^{11}B is a quadrupolar nucleus) that magnify the visualization of the processes that occur. We shall see that the trace features of the $^{11}B\{^1H\}$ NMR are not observed in the $^1H\{^{11}B\}$ NMR spectra, but other distinct information is drawn from there.

Changes in the relative chemical shifts for signals in the $^1H\{^{11}B\}$ NMR spectra of Na[**1**] with concentration and the assignment of B-H resonances have been reported earlier.[37b] In our work, the sharpness of the resonances in the $^1H\{^{11}B\}$ NMR spectra of H[**1**], Li[**1**], Na[**1**] and K[**1**] (Fig. 7), are quite similar irrespective of the concentration and the nature of the cation. Contrarily to the $^{11}B\{^1H\}$-NMR in which a better visualization with better definition of the signals is found at lower concentration, no major changes concerning these parameters is observed in the $^1H\{^{11}B\}$ NMR

spectra of H[**1**], Li[**1**], Na[**1**] and K[**1**]. This supports the adequacy of the $^{11}B\{^{1}H\}$ NMR spectra to study these solution phenomena. However, the $^{1}H\{^{11}B\}$ NMR spectra at increasing concentrations contribute complementary information to the one retrieved from the $^{11}B\{^{1}H\}$ NMR spectra in the same circumstances, and both data correlate with the phase transition. A close inspection to the $^{1}H\{^{11}B\}$ NMR spectra in Fig. 7 indicate that all resonances appear at the same position, independently of the cation and of the concentration, except the one at 4.0 ppm at 2.5 mM concentration. Indeed this resonance that corresponds to the C_c-H remains invariant in the concentration range 2.5 - 10 mM in which, the vesicles form but most of the [**1**]$^-$ is under monomeric form (i.e. non-aggregated), however, when the concentration reaches 20 mM at which concentration micelles are formed, the C_c-H resonance is shifted upfield for all salts. This is consistent with a phase transformation of the cobaltabisdicarbollide in which the highly hydrated monomeric form, forming B-H···H-O-H (and possibly C_c-H···O(H_2)) hydrogen bonds, is aggregated into the micellar form, in which C_c-H···H-B dihydrogen bonds are likely to be formed. On the contrary to C_c-H resonance, the influence of this weak interaction on the B-H resonances was not observed, probably because a large proportion of the B-H remains hydrated even after micellization whereas most C_c-H resonance are involved in the formation of dihydrogen bonds.

The IR spectrum of the H[**1**] / Li[**1**] / Na[**1**] salts of the anion [**1**]$^-$ in solid state display frequencies at 3591-3513 and 1641-1506 cm^{-1} that are related to the presence of coordinated water in addition to the ones in the range 2619-2513 cm^{-1} that are characteristic of the B-H stretching frequencies of the icosahedral Boron clusters (See S.I.).

2.4. NMR study of the H^+, and Na^+ salts of [I-1]$^-$ and [I_2-1]$^-$ in water.

The starting cesium salts of [3,3'-Co(8-I-1,2-$C_2B_9H_{10}$)(1',2'-$C_2B_9H_{11}$)]$^-$, ([I-**1**]$^-$) and [3,3'-Co(8-I-1,2-$C_2B_9H_{10}$)$_2$]$^-$, Cs[I_2-**1**], were prepared as previously reported. [42] [43]

It is also important to note that the $^{11}B\{^{1}H\}$ NMR spectrum of monosubstituted Cs[I-**1**] is the result of the addition of the two individual $[C_2B_9H_{11}]^{2-}$ η^5 ligands, as schematized in Fig. 8. Accordingly,

the $^{11}B\{^{1}H\}$ NMR of monosubstituted Cs[I-**1**] (at the bottom in Fig. 8) is the addition of the $^{11}B\{^{1}H\}$ NMR spectrum of the parent Cs[**1**] (in the middle) plus the $^{11}B\{^{1}H\}$ NMR spectrum of disubstituted Cs[I_2-**1**] (at the top). We had tested $^{11}B\{^{1}H\}$ NMR spectroscopy with other available examples of B(8) monosubstituted derivatives of [**1**]$^-$ and it works extremely well. [42], [44] This is therefore a remarkable tool to assist in the structural elucidation of derivatives of [**1**]$^-$ mainly when other techniques like COSY, GIAO are not applicable.

The H^+ and Na^+ salts of [I-**1**]$^-$ and [I_2-**1**]$^-$ were prepared by cation exchange, as described before, the corresponding $^{11}B\{^{1}H\}$ NMR studies in D_2O at different concentrations (See S.I.) were carried out in similarity to the $^{11}B\{^{1}H\}$ NMR studies done for [**1**]$^-$ (Fig. 6). The traces of the spectra at distinct concentrations of [I-**1**]$^-$ follow a trend very similar to the one observed in Fig. 6 for [**1**]$^-$ salts. From these studies, one may conclude that the monoiodinated species [I-**1**]$^-$ produces the phase transition at concentration higher that 15 mM for both, H^+ or Na^+, salts.

The $^{11}B\{^{1}H\}$ and $^{1}H\{^{11}B\}$ NMR spectra in D_2O of the H^+ and Na^+ salts of the disubstituted [I_2-**1**]$^-$ species were also run at different concentrations: 2.5, 5, 10, 20, 30 and 60 mM (Fig. 9). From the study of the $^{1}H\{^{11}B\}$ NMR spectra at different concentrations, it can be observed that the chemical shift of the C_c-H vertex remains unaffected, see Fig. 9b. Noticeably the other $^{1}H\{^{11}B\}$ NMR signals are not as sharp as these found in [**1**]$^-$ and [I-**1**]$^-$. Again the $^{11}B\{^{1}H\}$ NMR spectra, see Fig. 9a, is more informative, but not as much as for [**1**]$^-$ and [I-**1**]$^-$ as all signals are wider. It also shows the monomer/vesicles to micelles transition in the same range of concentration, above around 5-10 mM. Therefore the influence of the derivatization by iodine from [**1**]$^-$, to [I-**1**]$^-$ to [I_2-**1**]$^-$ does not influence significantly the critical micellization concentration, at least within the precision of the procedure used here to estimate critical micelle concentration (cmc ± 5 mM).

Further, the temperature dependent $^{11}B\{^{1}H\}$ NMR studies of 0.1 M and 1 M solutions of H[I_2-**1**] salt in aqueous and acetone solutions in the temperature range +20^{o}C / -60^{o}C was performed (Fig. 10 and 11). It was shown previously that lyotropic lamellar phases were formed by H[I_2-**1**] in

this concentration range and at temperatures below 10°C at 0.1M and below 30°C at 1M. [17c] It is observed that the solvent (H_2O or acetone) and the metallacarborane concentration influences both the color of the solutions as well as the NMR spectra. It should be noted that the lamellar phases formed by [I_2-**1**]$^-$ are in crystalline state, as clearly seen in the SWAXS spectra, [17c] and can therefore not be seen with liquid NMR. In the previous investigation by Brusselle et al. it was shown that the lyotropic lamellar phase (L_β) forms in equilibrium (coexistence) with a micellar phase (L_1). As a consequence, the liquid NMR performed here informs on the liquid state of [I_2-**1**]$^-$, i.e. as monomers and as micelles.

The temperature dependence $^{11}B\{^1H\}$-NMR of 0.1 M and 1 M solutions of H[I_2-**1**] salt in aqueous (Fig. 10 and 11) produces again ill defined spectra, as expected for [I_2-**1**]$^-$ micelles, that worsen by decreasing T. The decrease in T reinforces the formation of lyotropic lamellar, as seen in the water/[I_2-**1**]$^-$ phase diagram. [17c] As a consequence, the decrease in the quality of the NMR resonances by decreasing temperature can be associated to the decrease in the concentration of micelles in favor of the formation of lamellar phase. On the contrary the $^{11}B\{^1H\}$ NMR in acetone at 0.1 M produces well defined signals (Fig. 12), which is not surprising as acetone is known to disassemble aggregates in monomers, that are not affected by lowering temperature. However at 1M in acetone, the NMR resonances become broader for temperature below -20°C which is possibly due to an aggregation process, such as lamellar phase formation (see Fig. 11). Interestingly, this informs on the strong tendency of [I_2-**1**]$^-$ to self-assemble even in highly destructuring solvents such as acetone.

To lightening on the interactions between adjacent [I_2-**1**]$^-$ clusters, a search at the Cambridge Structural Database (CSD) [45], [29b] was done: 4 hits (codes DEXPIF, [46] IHOHAP, [9a] IHOHET, [9a] and IHOHIX [9a]) were found that contain [I_2-**1**]$^-$ clusters. In all of them the [I_2-**1**]$^-$ ions present a two-fold symmetry with the two iodine atoms in *trans* position, as shown in Fig. 1, which represents the *transoid* conformer being the most stable. The presence of intermolecular B-

$H^{\delta+}\cdots^{\delta-}$H-B dihydrogen bonds of 3.500 Å are observed in the solid state for the [BEDT-TTF][I_2-**1**] (CSD code IHOHAP) [9a] (see S.I.), which matches with the 2D arrangement separation found in the lamellae phase of H[I_2-**1**]. [17c]

2.5. Computational analysis of the intramolecular interactions

At the first stage, separate single anionic species [**1**]$^-$ and [I_2-**1**]$^-$ were studied to reveal possible intramolecular interactions, which could affect the final structure of the complexes and their self-assembly. The two dicarbollide cages can take different conformations when bonding to metal ions in the dicarbollide complexes. Fig. 13 shows the different options in the [I_2-**1**]$^-$ rotamers, which were fully optimized at the DFT level of theory and the possible intramolecular interactions studied with the QTAIM methods. The obtained bond paths and bond critical points as well as relative total energies are reported in Fig. 13.

In both complexes, the *transoid* conformer with the carbon atoms at the opposite sides of the two dicarbollide ligands was energetically the most favorable one. The same energetic preference was found in a previous computational study, which used a different density functional method for optimizing the [**1**]$^-$ structures. [22] However, in [**1**]$^-$ anions *gauche* and *cisoid* conformers showed rather similar stability, which would make them feasible in suitable experimental conditions. In [I_2-**1**]$^-$, the *transoid* conformer was clearly preferred, and especially the *cisoid* conformer was about 66 kJmol^{-1} less favorable, indicating that this structure is less likely to be found in the crystal structure of the compounds. Experimentally, [**1**]$^-$ crystallizes as *cisoid* conformers, but [I_2-**1**]$^-$ as the *transoid* conformer, which is in agreement with the relative total energies.

In the case of [I_2-**1**]$^-$, there are additional weak intramolecular interactions between iodine and C_c-H hydrogens (Fig. 13), which further stabilize the structure, and determine the relative orientation of the two cage ligands in the molecule, therefore affecting the self-assembly. Table 1 lists the properties of the intramolecular interactions in the different conformers of the [I_2-**1**]$^-$ molecular model according to the QTAIM analysis.

The intramolecular interactions consist of hydrogen bonding of either B-H···I-B or C_c-H···I-B. The properties of the interactions shown in Table 1 indicate that both interactions are clearly non-covalent in nature because of the small value of electron density at the corresponding BCPs, and the |V|/G value is less than 1. [47] The positive Laplacian (second derivative of electron density) shows depletion of electron density at the bond critical point, again typical for non-covalent interactions. Small interaction energy corresponds to weak hydrogen bonding interactions. Notably, the C_c-H···I-B interaction is slightly stronger than the B-H···I-B one, which can be one reason for the larger stability of the *transoid* conformer, since all the intramolecular interactions originate from the C_c-H in this conformer. On the other hand, in the *cisoid* conformer the iodines are located too far from the carbon atoms to form C_c-H···I-B interactions, and consequently the *cisoid* conformer is the least favorable of the $[I_2$-**1**$]^-$ structures.

Intramolecular interactions have a clear effect on the total atomic charges of iodine atoms in the different conformers. Even though the charge of the interacting hydrogen atoms remain rather constant, the negative charge of iodine increases in the order of *cisoid* < *gauche* < *transoid*. This is a result of change in the nature of the intramolecular interactions from B-H···I-B to C_c-H···I-B, where the latter was also found energetically stronger. Interestingly, the positive charge of the central cobalt also increases in the same order. These subtle changes in the charge distribution are potential sources of various intermolecular interactions, when the molecules assemble into aggregates.

2.6. Computational analysis of the intermolecular interactions and self-assembly

To study the weak intermolecular interactions in the molecular assemblies of the [**1**]$^-$ and $[I_2$-**1**$]^-$ structures, we analyzed the charge densities for models presented in Fig. 14, which show the 2-unit models together with the shortest intermolecular interactions. The analysis of the intermolecular interactions was done with non-optimized models cut directly from the experimental crystal structures (QOLVES [32] in the case of [**1**]$^-$, and IHOHAP [9a] in the case of $[I_2$-**1**$]^-$). The models

consisted of two adjacent anionic complexes and the counter ions were omitted, since the focus was in the hydrogen bonding interactions between the complexes. Table 2 lists the selected properties of the electron density at the corresponding bond critical points for interactions shown in Fig. 14.

According to the QTAIM analysis, all intermolecular interactions are non-covalent and very weak. It should be noted that Table 2 shows only the shortest intermolecular interactions, while the full view of the interactions present in the solid state structures is shown at the supporting information (Figures S1-S5). Especially in the $[I_2\text{-}\mathbf{1}]^-$ cluster, the interactions are far more complicated than have been shown above in Fig. 14. Therefore, even though the hydrogen bonding interactions between the iodine substituted complexes were somewhat weaker than in the parent model, the additional B-H···H-B and B-H···I-B interactions were able to stabilize the structure.

The electrostatic nature of the intermolecular interactions can be seen when the total atomic charges are compared for interacting hydrogen atoms in the 2-unit models. As can be expected, the hydrogen atom attached to boron, H_B, shows a negative partial charge, opposite to the hydrogen atom attached to carbon (H_C), which is clearly positive, giving a relative charge distribution of B-$H_B^{\delta-}\cdots^{\delta+}H_C$-$C_c$.

Intermolecular B-H···H-C_c interaction was found to diminish both the positive charge of H_C and the negative charge of H_B in the previous computational study of the $[\mathbf{1}]^-$ crystal structure. [22] Similar trends can also be seen in our compounds, when compared to the charges obtained for the separate molecules. When the H_C and H_B charges are compared between the monomers (Table 1) and dimers (Table 2), it can be noted that the intermolecular B-H···H-C_c interactions indeed include charge transfer between the molecules. The B-H···H-B interactions do not have similar effect on the charge distribution, therefore indicating weaker dispersion interactions. However, there is obviously a summarized effect of the weak interactions, since the larger number of the interactions will lead to larger stabilization of the molecular assembly in the solid state.

The extended 4-unit models of [**1**]$^-$ and [I_2-**1**]$^-$ were also studied to find out more on the role of intermolecular interactions in self-assembly and crystal packing (Figs.S3 and S4). In [**1**]$^-$, there are discrete chains of molecules, and the chains do no interact directly. Because the complexes are found in the *cisoid* conformer in the crystalline state, the 2D assemblies are not preferred like they are in the more symmetrical *transoid* conformer of complex [I_2-**1**]$^-$ in the solid state. Furthermore, in [I_2-**1**]$^-$, there are additional hydrogen bonding interactions, which make the molecules to arrange in 2D layers. The iodine substituent seems to have an important role in determining the self-assembly, since they are forming additional weak interactions not with the counter ions but with adjacent complexes. The symmetrical 2D arrangement is also a result of having the iodine substituent symmetrically pointing out in opposite directions, ie. in *transoid* conformation.

In addition, the role of the Na^+ counter ion in the self-assembly of the [**1**]$^-$ anions was studied by analyzing the intermolecular interactions present in the crystal structure of $[Na(H_2O)_4][Co(C_2B_9H_{11})_2]$ (code XUXMOU). [33] The model with the numbering of the bond critical points is presented in Fig. S5, and the properties of the electron density at the selected BCPs according to the QTAIM analysis is shown in Table 3. In water solution, Na^+ ions naturally form solvated structures, and in the crystal structure, the fairly strong electrostatic $Na^{\cdots}OH_2$ interactions (E_{INT} = -21 kJmol^{-1}) remain, forming $Na(H_2O)_4$ chains with octahedrally coordinated Na^+ ions. The [**1**]$^-$ anions self-assemble around the counter ions in a layered structure *via* several B-H$^{\cdots}$H-O bonds, the strength of which is comparable with the ones obtained for the intermolecular dihydrogen bonds found between the adjacent anions in the chain-like structure of [**1**]$^-$ (QOLVES, Table 2). This indicates that the dihydrogen-bonding interactions with the counter ions have a co-operative influence on the self-assembly of the dicarbollide complexes together with the B-$H_B^{\delta-}\cdots^{\delta+}H_C$-$C_c$ bonds between adjacent anions.

3. Conclusions:

Salts of Na^+, K^+ and Li^+ of cobaltabisdicarbollide [**1**]$^-$ were prepared by cation exchange as an advanced alternative to the extraction procedure in diethyl ether that leads primarily to the protonated cobaltabisdicarbollide. The study of the available crystal structures has revealed the intermolecular dihydrogen B(8)-H(8)···H-O interaction, in which the H_2O molecule is at the Na^+ coordination sphere. Further, the cluster C_c-H units in [**1**]$^-$ are ready to generate B-H···H-C_c dihydrogen bonds. The presence of both B-H and H-C_c bonds in the structure of [**1**]$^-$ is likely to be responsible for the formation of intermolecular dihydrogen bonds that produce aggregates of [**1**]$^-$ in water. When these assemblies are surrounded by water molecules, they adopt a stable conformation that avoids the direct contact of the connecting non-bonding interactions with water generating supramolecular entities. This is observed in the $^{11}B\{^1H\}$ NMR of M[**1**] (M= alkali or H^+) in water that exhibits much wider signals than in an organic solvent that causes disaggregation. The wider resonances are found at concentrations larger than 10 mM, but as expected the more sharp signals are found at lower concentrations. At concentrations lower than 10 mM vesicles had been observed with other techniques like CryoTEM or SANS. This seemed to be in contradiction as the widening of the signals can be interpreted by tumbling motions of the aggregates affecting the $^{11}B\{^1H\}$ NMR relaxation data at various concentrations of [**1**]$^-$. However, these data corroborate other information from the SANS investigation on the self-assembly of H[**1**] in water that concluded that below 10 mM a large fraction of H[**1**] is under monomeric form and only a small fraction of H[**1**] participate the formation of vesicles. Therefore the $^{11}B\{^1H\}$ NMR of H[**1**] at concentrations lower than 10 mM corresponds to the monomer and that the phase transition is due to the monomer to micelles transformation. Another remarkable feature obtained from the $^{11}B\{^1H\}$ NMR of all alkaline salts and proton suggests that the phase transition between vesicles/monomer and micelles appears between 10 and 20mM, for all tested cations. The $^{11}B\{^1H\}$ NMR is, therefore, an excellent probe to visualize the processes that occur. The $^1H\{^{11}B\}$ NMR spectra at increasing concentrations contribute interesting complementary information to the one retrieved from the $^{11}B\{^1H\}$ NMR,

particularly in what concerns B-H···H-O-H (and possibly C_c-H···O(H_2)) hydrogen bonds, in which C_c-H···H-B dihydrogen bonds are likely to be formed.On the other hand, the traces of the spectra at distinct concentrations of [I-**1**]$^-$ follow a trend very similar to this observed for [**1**]$^-$ salts indicating that similar phase transitions occur although at slightly different concentrations higher than 15 mM for both, H^+ or Na^+, salts. It is then found that the derivatization by iodine from [**1**]$^-$, to [I-**1**]$^-$ to [I_2-**1**]$^-$ does not influence significantly the critical micellization concentration, at least within the precision of the procedure used here to estimate critical micelle concentration (cmc ± 5 mM).

Overall, the intermolecular B-$H_B^{\delta-}$···$^{\delta+}H_C$-C interactions can be suggested to have a major role in the formation of the self-assembly of the cobaltabisdicarbollide anions in aggregates. The number of the intermolecular interactions is affected by the differences in the conformational molecular structure, especially in the case of large substituents capable of polarizing the charge, such as iodine. Intramolecular I···H-C interactions lead to preferred *transoid* rotamer in [I_2-**1**]$^-$, which can in turn form B-H···I-B hydrogen bonds between adjacent molecules and, consequently, 2D layers leading to a lamellar arrangement of the molecules. On the other hand, the stronger intermolecular B-H···H-C interactions in the *cisoid* rotamer of [**1**]$^-$ facilitate the assembly of the molecules in the chain-like manner, therefore leading to vesicle formation. On the other hand, the self-assembly can also be affected by the coordination of the counter ions, as was found to be the case in the crystal structure of $[Na(H_2O)_4][Co(C_2B_9H_{11})_2]$, where a layered 2D structure was formed instead of a 1D chain.

4. Experimental section:

Cs[**1**] was from Katchem and it was used as received. [NMe_4][I-**1**] and [NMe_4][I_2-**1**] were synthesized from Cs[**1**] as reported at the literature.[42] [43]

The Na[**1**] was obtained by means of cationic exchange resin from Cs[**1**]. Approximately 2/3 of the volume of the column (30 cm) was filled by the strongly acidic cationic exchange resin (Amberlite IR120, H form). Before starting, the cationic resin was kept 24 h in HCl 3 M to hydrate it. Then, 150 mL solution of HCl 3M was slowly passed through the column to load it with H^+. To remove

the excess of HCl, distilled water flows down the column fast till neutral pH. When the desired cation was sodium, a solution of NaCl 3M was passed through the column slowly to exchange H^+ by Na^+ till neutral pH. Distilled water was used to rinse the excess of NaCl through the column. To know if NaCl was removed, 3 drops of a solution of $AgNO_3$ 100 mM was added to a small fraction of solution coming out of the column until a clear solution is observed. Then, 30 mL of acetonitrile/water (50:50) mixture was flown through the column to set the column's liquid composition. Approximately 200 mg of Cs[**1**] was dissolved in a minimum volume of acetonitrile/water (50:50) and let to go repeatedly (4 times) through the cationic resin. Before collecting the solution containing the metallacarborane, 50 mL of fresh acetonitrile/water (50:50) was added to the column. 50 mL were collected in a flask, the solvent was evaporated and the compound was dried in vacuum. The Na[I-**1**] and Na[I_2-**1**] salts were obtained by means of cationic exchange resin from [NMe_4][I-**1**] and [NMe_4][I_2-**1**].

The Li[**1**] and K[**1**] was obtained also by means of cationic exchange resin from Cs[**1**]. The same procedure as Na[**1**] but instead of loading the column with NaCl 3 M, solutions of LiCl 3 M and KCl 3 M were, respectively, used.

The H[**1**], H[I-**1**] and H[I_2-**1**] were obtained by liquid-liquid extraction from Cs[**1**], [NMe_4][I-**1**] and [NMe_4][I_2-**1**], respectively. Approximately 200 mg of Cs[**1**] was dissolved in 20 mL diethyl ether. The sample was transferred to a separatory funnel and 15 mL HCl 1 M was added. Two phases were formed and by shaking the metallacarborane sample passed through the organic layer. The organic layer was shaked three times with HCl 1 M (3x 15 mL) to change completely Cs^+ to H^+. The metallacarborane was collected in a flask and dried with anhydrous $MgSO_4$ to remove residual water. Then, the ether slurry was filtered, the diethyl ether was evaporated and the compound was dried in vacuum. The ^1H NMR spectra of the salts H[I-**1**], Na[I-**1**], H[I_2-**1**] and Na[I_2-**1**] do not display the peak at ppm that corresponds to the $[NMe_4]^+$ being a clear evidence of the absence of $[NMe_4]^+$.

Instrumentation. The ^1H, $^{11}B\{^1H\}$ and $^1H\{^{11}B\}$ NMR (300.13 MHz) and ^{11}B and $^{11}B\{^1H\}$ NMR (96.29 MHz) spectra were recorded on a Bruker ARX 300 instrument equipped with the appropriate decoupling accessories. All NMR spectra were performed in D_2O or acetone deuterated solvents at 22ºC except the dynamic studies. The ^{11}B and $^{11}B\{^1H\}$ NMR shifts were referenced to external $BF_3{\cdot}OEt_2$, while the ^1H and $^1H\{^{11}B\}$ NMR shifts were referenced to $SiMe_4$. Chemical shifts are

reported in units of parts per million downfield from the reference. IR spectra (ν, cm-1; ATR) were recorded on a Shimadzu FTIR-8300 spectrophotometer.

CryoTEM sample was prepared from a 1 mM aqueous solution of Na[**1**]. Vitrified specimens were prepared by placing 3 μL of the sample suspension on a 400 mesh copper grid with a holey carbon support. Each sample was blotted to a thin film and immediately plunged into liquid ethane in the Leica CPC cryoworkstation. The grids were viewed on a JEOL 2011 transmission electron microscope operating at an accelerating voltage of 200 kV. The microscope was equipped with a Gatan cryoholder and the samples were maintained at -177ºC during imaging. Electron micrographs were recorded with the Digital Micrograph software package under low electron dose conditions, to minimize electron bean radiation. Images were recorded on a Gatan 794 MSC 600HP cooled charge-coupled device (CCD) camera.

Computational methods and models.

All models were calculated with the Gaussian 09 program package [48] at the DFT level of theory. The hybrid density functional PBE0 [49] was utilized together with the basis set consisting of the def2-TZVPPD [50] triple-zeta-valence basis set with two sets of polarization and diffuse basis functions for Co atoms and the standard all-electron basis set 6-31G(d,p) for all other atoms. To study the electronic and interaction properties of the complexes, we performed topological charge density analysis with the QTAIM (Quantum Theory of Atoms in Molecules) [51] method, which allowed us to access the nature of the bonding via calculating different properties of the electron density at the bond critical points. The analysis was done with the AIMAll program [52] using the wave functions obtained from the DFT calculations. The models for the solid state structures were directly cut from the corresponding experimental crystal structures and analyzed without geometry optimization.

Supporting Information

The Supporting Information includes the full characterization of the reported compounds (H[**1**], Li[**1**], Na[**1**], K[**1**], Na[I-**1**], Na[I_2-**1**]); $^{11}B\{^1H\}$-NMR study in D_2O of the H[I-**1**], Na[I-**1**] at different concentrations (5, 10, 15, 20, 25 and 30 mM); $^{11}B\{^1H\}$ NMR dynamic study of 0.1M and 1M aqueous solutions of **H[I_2-1]** in the temperature ranges 50ºC / 12ºC and 23ºC / -10ºC, respectively; $^{11}B\{^1H\}$ NMR dynamic study of 0.1M and 1M solutions of **H[I_2-1]** in acetone into the temperature ranges 23ºC / -50ºC and 23ºC / -60ºC, respectively; a view of the crystal packing of [BEDT-TTF]$_2$[I_2-**1**] (CDS code IHOHAP) displaying the B-H···H-B intermolecular interactions. Figures of bond paths and bond critical points in the 2-unit model of [**1**]$^-$, in the 2-unit model of [I_2-**1**]$^-$, in the 4-unit model of [**1**]$^-$, in the 4-unit model of [I_2-**1**]$^-$ and in the 4-unit model of [**1**]$^-$ with Na^+ counter ions surrounded with water molecules.

Acknowledgements

The authors would like to acknowledge support from the Spanish Ministerio de Economía y Competitividad CTQ2013-44670-R, and the Generalitat de Catalunya (2014/SGR/149) and the European Network on Smart Inorganic Polymers (SIPs) COST CM1302 project. Grants of computer capacity from the Finnish Grid and Cloud Infrastructure (persistent identifier urn:nbn:fi:research-infras-2016072533) are also gratefully acknowledged.

Figure 1. Icosahedral numbered metallacarboranes [3,3'-Co(1,2-$C_2B_9H_{11})_2]^-$, [**1**]$^-$, and [3,3'-Co(8-I-1,2-$C_2B_9H_{10})_2]^-$, [I_2-**1**]$^-$.

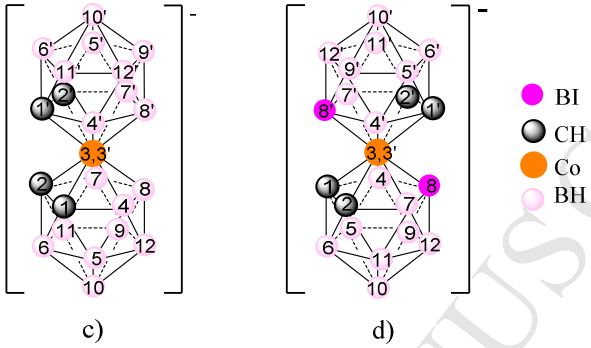

Figure 2. Packing of the [Na[2.2.2]cryptand][**1**] with the formation of [**1**]$^{-}$ aggregates stabilized by double intermolecular dihydrogen bonds, shown as dashed lines. The figure is adapted from the reported crystal structures. [32]

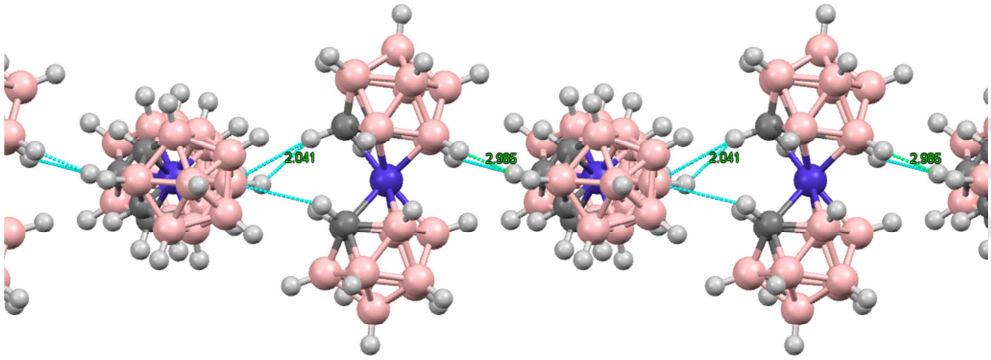

Figure 3. Packing of the $[Na(H_2O)_4][\mathbf{1}]$: a) displays the Na^+ forming a 1D chain through axis *b* and b) that each Na^+ is surrounded by four $[\mathbf{1}]^-$ anion clusters through the axis *a* structure in which the blue lines display van Der Waals interactions shorter than sum of vdW radii – 0.30 Å that correspond to B(12)-H(12)···H-O and B(10)-H810)···HO. c) The blue lines display van Der Waals interactions shorter than sum of vdW radii – 0.40 Å that correspond to B(8)-H(8)···H-O of two molecules. The figure is adapted from the reported crystal structure (CDS code XUXMOV). [33]

a)

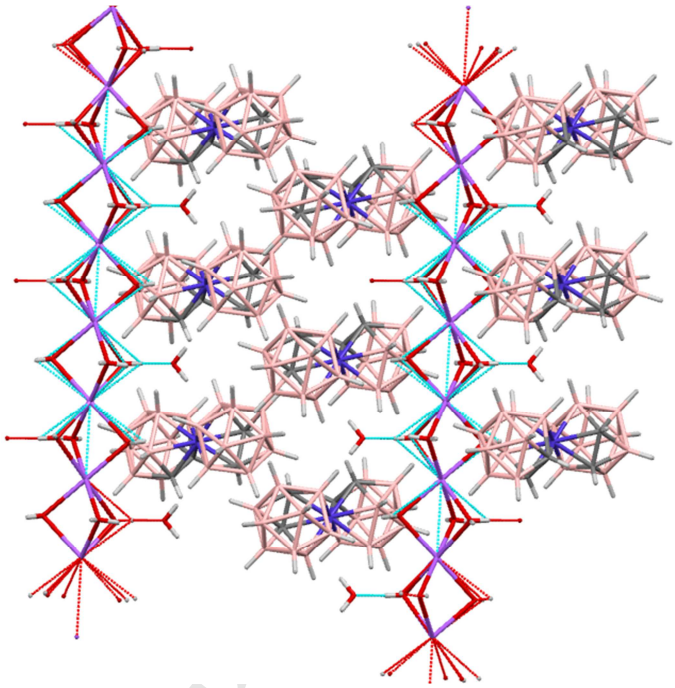

b

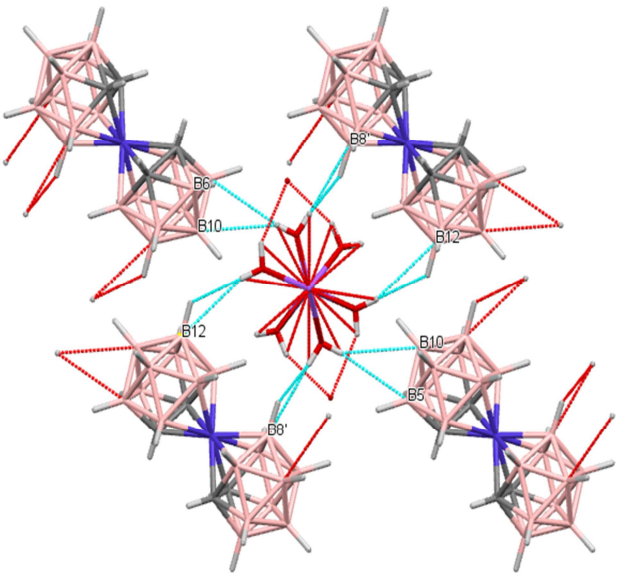

c)

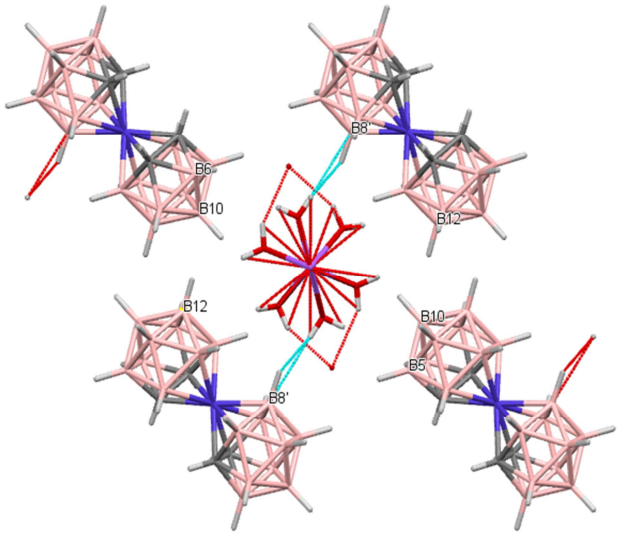

Figure 4. Representation of the monolayer vesicles of cobaltabisdicarbollide anion, [**1**]$^-$.

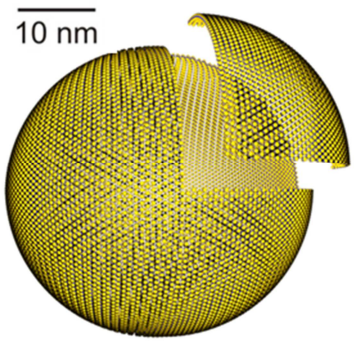

Figure 5. Visualization by Cryo-TEM of the hollow structure of the Na[**1**] vesicles from a 1 mM aqueous solution. The depicted part of the figure corresponds to the holey carbon support.

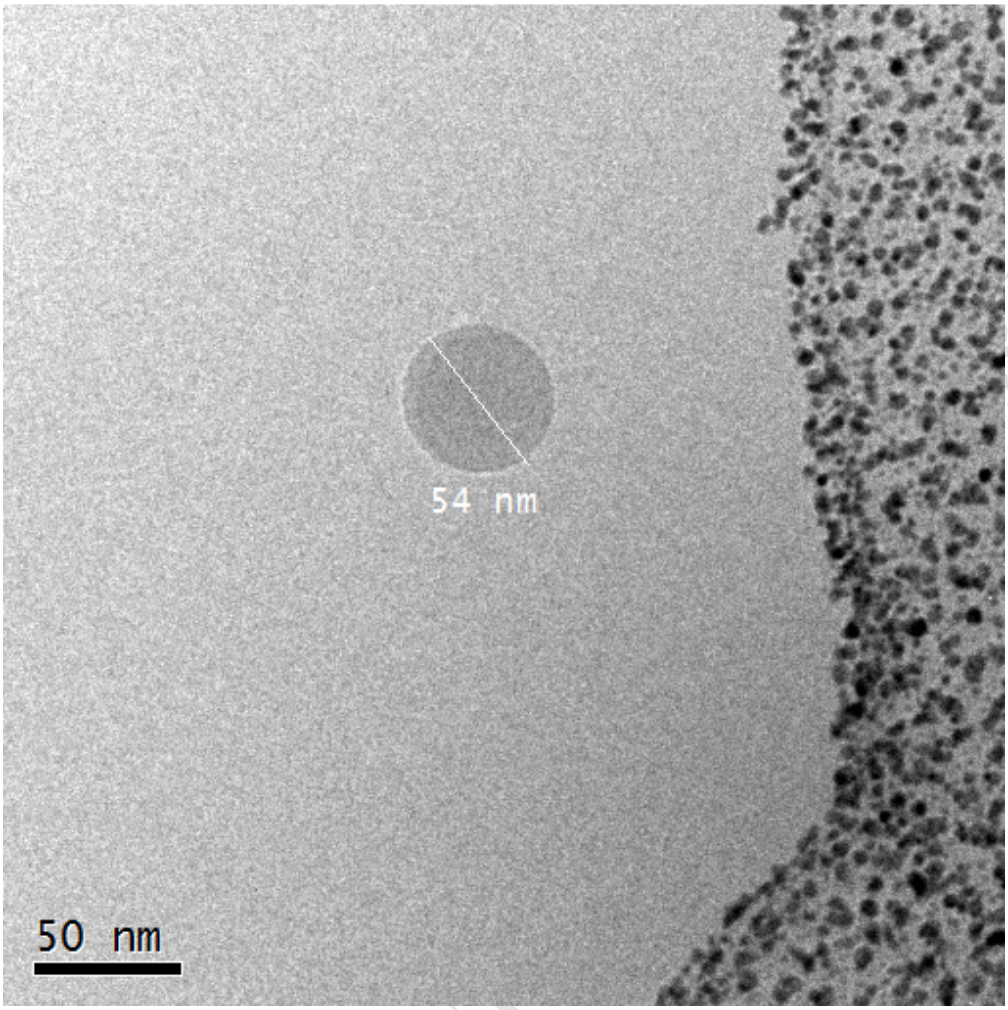

Figure 6. $^{11}B\{^{1}H\}$ NMR studies in D_2O of the H[**1**], Li[**1**], Na[**1**] and K[**1**] at different concentrations: 2.5 mM (in pale green), 5 mM (in black), 10 mM (in green), 20 mM (in purple), 30 mM (in blue) and 60 mM (in red).

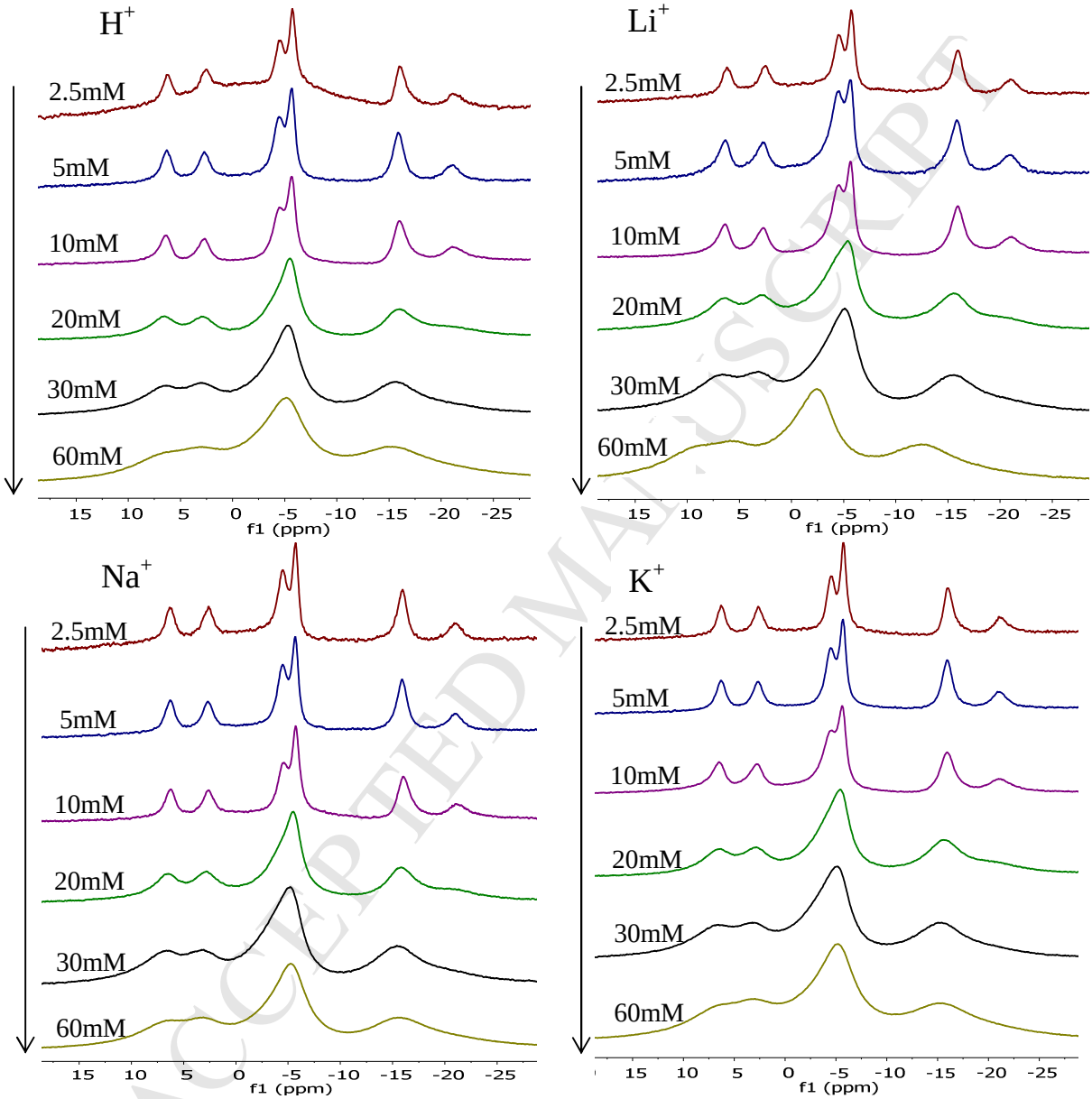

Figure 7. $^{1}H\{^{11}B\}$ NMR studies in D_2O of the H[**1**], Li[**1**], Na[**1**] and K[**1**] at different concentrations: 2.5, 5, 10, 20, 30 and 60 mM.

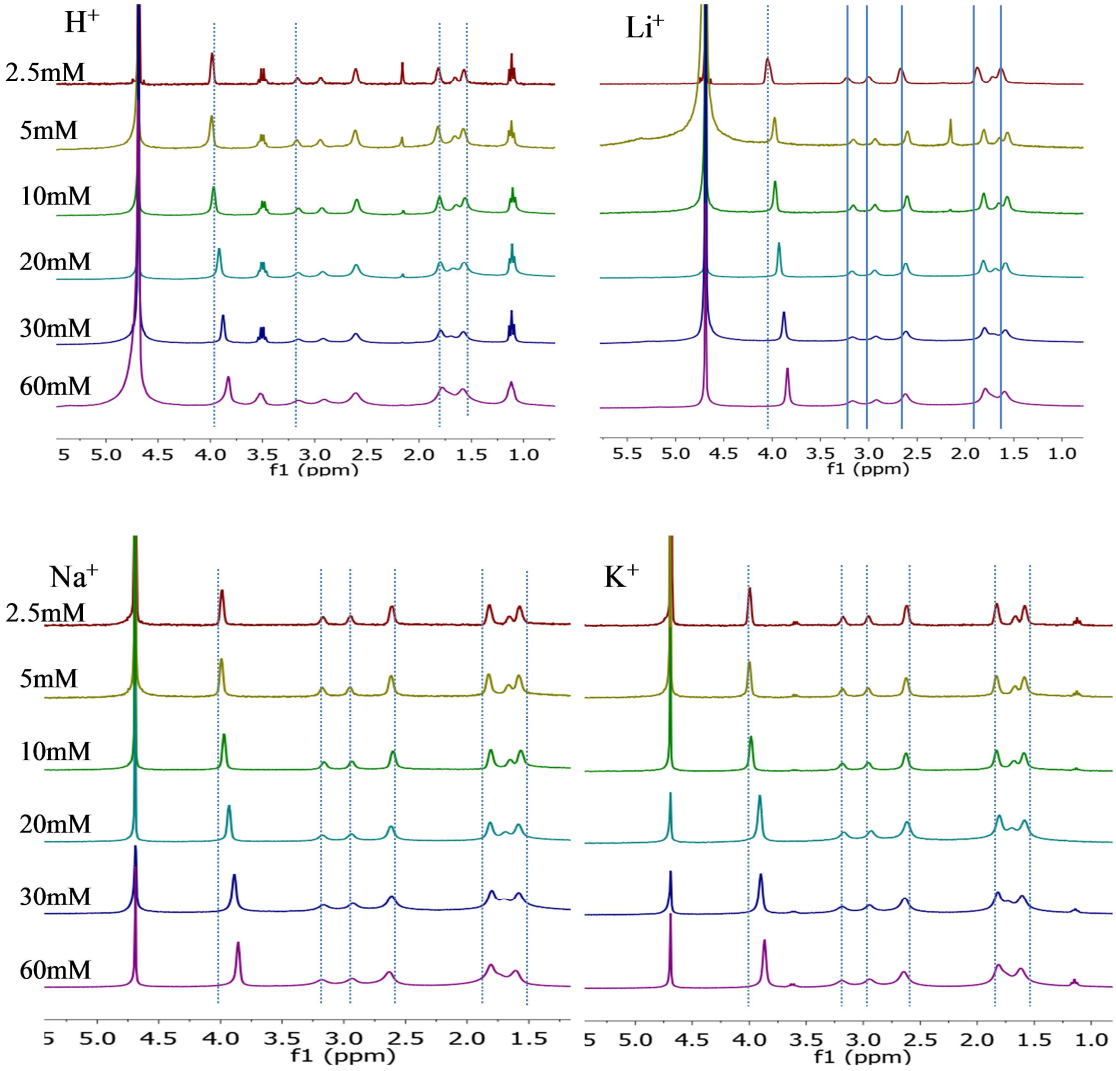

Figure 8. $^{11}B\{^{1}H\}$ NMR spectra of $[I_2\text{-}\mathbf{1}]^-$ (in red), $[\mathbf{1}]^-$ (in blue), $[I\text{-}\mathbf{1}]^-$ (in green) run in acetone.

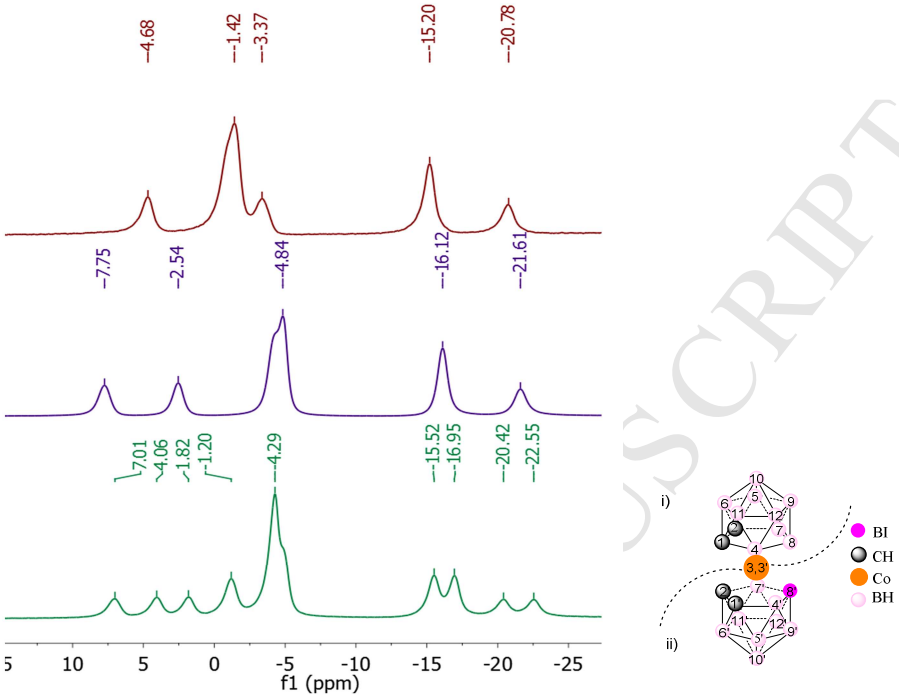

Figure 9. $^{11}B\{^{1}H\}$ and $^{1}H\{^{11}B\}$ NMR spectra in D_2O of the Na[I_2-**1**] at different concentrations (2.5, 5, 10, 20, 30 and 60 mM).

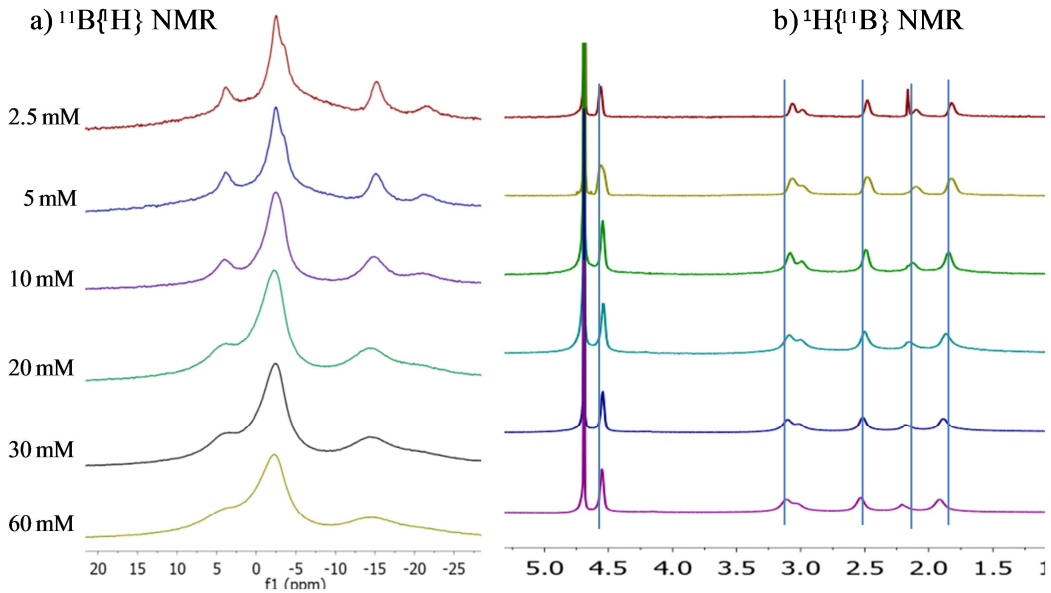

Figure 10. $^{11}B\{^{1}H\}$ NMR dynamic study of a 0.1M solutions of H[I_2-**1**] in aqueous (left) and acetone (right) media in the range +20ºC/-10ºC.

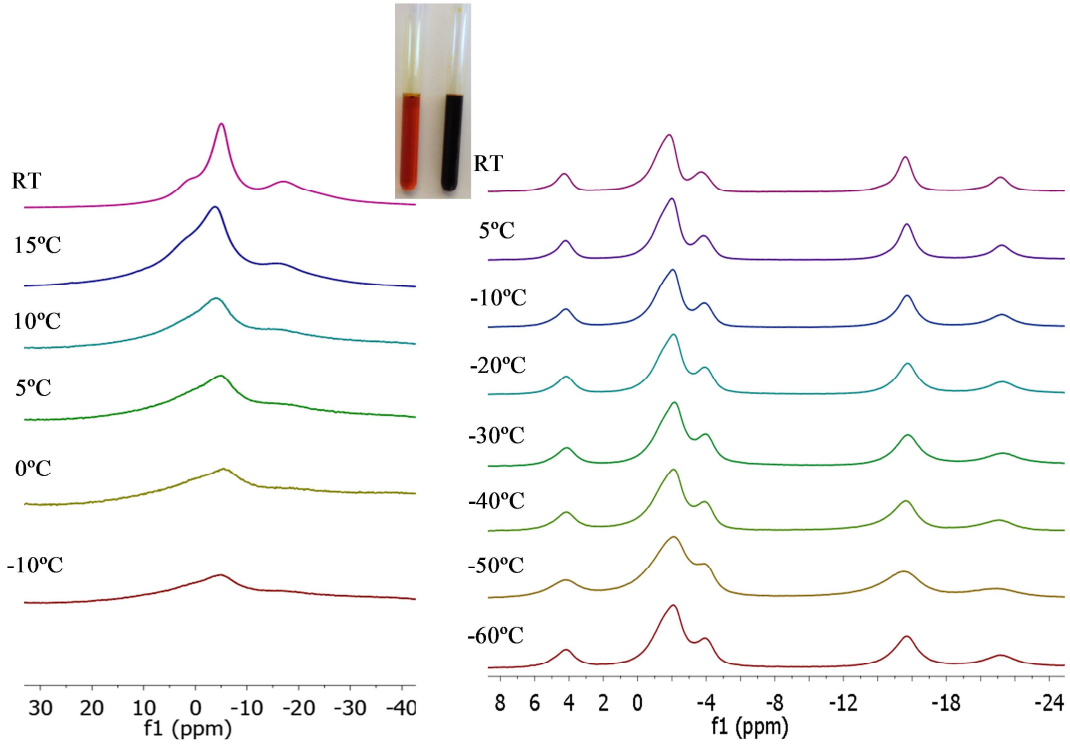

Figure 11. $^{11}B\{^{1}H\}$ NMR dynamic study of a 1M solutions of H[I_2-**1**] in aqueous (left) and acetone (right) media.

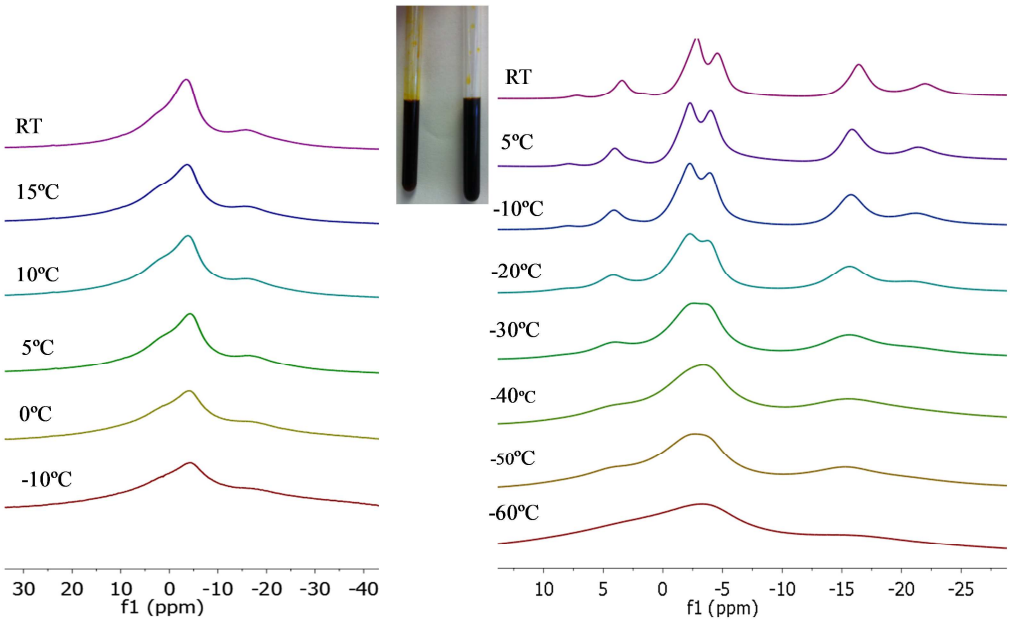

Figure 12. $^{11}B\{^{1}H\}$ NMR spectra at room temperature of a 0.1 M solution of H[I_2-**1**] in water (black) and in acetone (red).

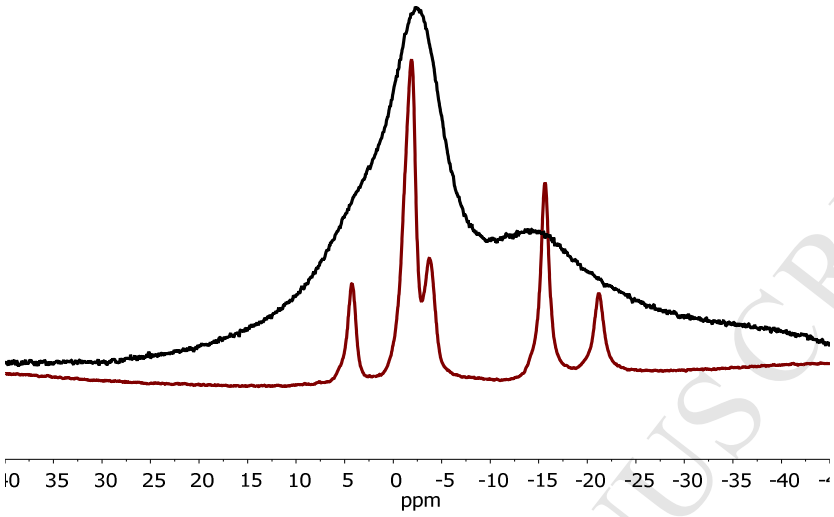

Figure 13. Intramolecular interactions present in the different rotamers of the $[I_2\text{-}\mathbf{1}]^-$ structure. Bond paths and bond critical points (BCPs) are calculated according to QTAIM method. Corresponding numbering of the BCPs is used also in Table 1. Color scheme: blue = Co, gray = C_c, pink = B, white = H, purple = I.

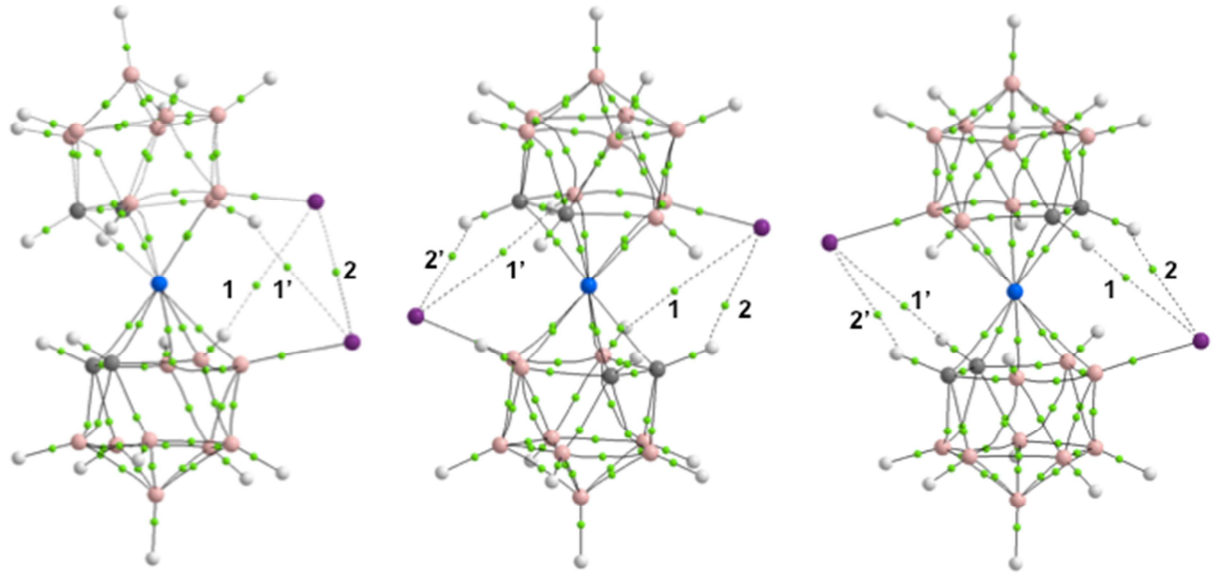

	cisoid	gauche	transoid
$[\mathbf{1}]^-$	15.7 kJmol^{-1}	3.5 kJmol^{-1}	0.0 kJmol^{-1}
$[I_2\text{-}\mathbf{1}]^-$	65.9 kJmol^{-1}	19.7 kJmol^{-1}	0.0 kJmol^{-1}

Figure 14. Two-unit models for the [**1**]$^-$ (a) and [I_2-**1**]$^-$ (b) structures. The shortest hydrogen-bonding interactions (predicted by QTAIM) are shown as green dashed lines. Numbering of the interactions is followed in Table 2. Color scheme: blue = Co, gray = C_c, pink = B, white = H, purple = I.

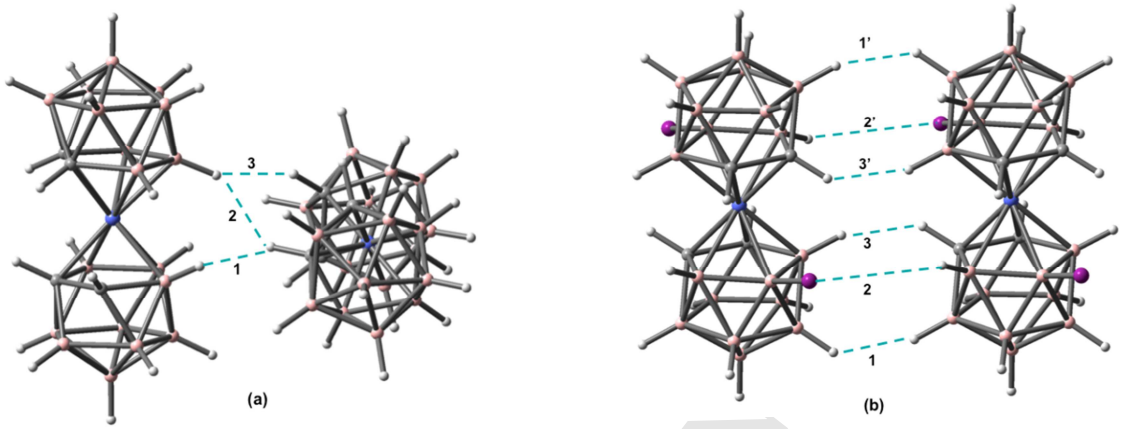

Table 1. Properties of the electron density according to the QTAIM analysis at the corresponding bond critical points (BCPs) in the different rotamers of the $[I_2$-**1**$]^-$ structure. The selected properties are: d=distance between interacting atoms; ρ = local electron density at the BCP; Laplacian ($\nabla^2 \rho$) = second derivative of ρ; |V|/G = ratio of potential energy density and kinetic energy density; E_{INT} = interaction energy between two interacting atoms; $q(H_B)$ = total atomic charge of hydrogen atom attached to B; $q(H_C)$ = total atomic charge of hydrogen atom attached to C, q(I)= charge of iodine, q(Co)= charge of cobalt.

BCP#	type	d(Å)	ρ(eÅ^{-3})	$\nabla^2\rho$(eÅ^{-5})	|V|/G	E_{INT}(kJmol^{-1})	$q(H_B)$	$q(H_C)$	q(I)	q(Co)
	cisoid									
1	B-H…I-B	3.030	0.067	0.701	0.78	-6.2	-0.590		-0.374	0.564
2	B-I…I-B	3.952	0.060	0.474	0.87	-5.0			-0.374	
	gauche									
1	B-H…I-B	3.223	0.053	0.566	0.76	-4.8	-0.590		-0.406	0.577
2	C-H…I-B	2.854	0.082	0.856	0.85	-8.6		0.109	-0.406	
	transoid									
1	C-H…I-B	2.909	0.076	0.798	0.84	-7.8		0.108	-0.421	0.598
2	C-H…I-B	2.909	0.076	0.798	0.84	-7.9		0.108	-0.421	

Table 2. Properties of the electron density according to the QTAIM analysis at the BCPs of intermolecular interactions in the two-unit models of $[$**1**$]^-$ and $[I_2$-**1**$]^-$. The selected properties are: d=distance between interacting atoms; ρ = local electron density at the BCP; Laplacian ($\nabla^2 \rho$) = second derivative of ρ; |V|/G = ratio of potential energy density and kinetic energy density; E_{INT} = interaction energy between two interacting atoms; $q(H_B)$ = total atomic charge of hydrogen atom attached to B; $q(H_C)$ = total atomic charge of hydrogen atom attached to C.

BCP#	type	d(Å)	ρ(eÅ^{-3})	$\nabla^2\rho$(eÅ^{-5})	|V|/G	E_{INT}(kJmol^{-1})	$q(H_B)$	$q(H_C)$
				$[$**1**$]^-$				
1	B-H…H-C	1.972	0.083	1.066	0.79	-9.6	-0.662	0.097
2	B-H…H-C	2.247	0.046	0.563	0.71	-4.2	-0.684	0.097
3	B-H…H-C	2.267	0.042	0.495	0.70	-3.7	-0.684	0.086
				$[I_2$-**1**$]^-$				
1	B-H…H-B	2.444	0.034	0.406	0.63	-2.5	-0.668	-0.650[a]
2	B-H…I-B	3.357	0.038	0.387	0.69	-2.8	-0.673	-0.405[b]
3	B-H…H-C	2.455	0.028	0.346	0.62	-2.1	-0.668	0.127

[a] hydrogen at the second B; [b] iodine charge

Table 3. Properties of the electron density according to the QTAIM analysis at the BCPs of intermolecular interactions in the 4-unit model of $[\mathbf{1}]^-$ with $(Na(H_2O)_4)^+$ counter ions. The numbering scheme of the BCPs is presented in Fig. S5.

BCP#	type	d(Å)	$\rho(eÅ^{-3})$	$\nabla^2\rho(eÅ^{-5})$	|V|/G	$E_{INT}(kJmol^{-1})$
1	B-H…H-O	1.954	0.072	0.954	0.83	-9.2
2	B-H…H-O	2.251	0.043	0.636	0.71	-4.7
3	B-H…O-H	2.408	0.029	0.454	0.67	-3.1
4	B-H…H-O	2.319	0.040	0.648	0.69	-4.6
5	Na…O-H	2.408	0.112	2.315	0.81	-21.3
6	O…O	3.162	0.039	0.533	0.90	-5.9

References

[1] a) A. K. Saxena, N. S. Hosmane, Chem. Rev. 93 (1993) 1081;

A. K. Saxena, J. A. Maguire, N. S. Hosmane, Chem. Rev. 97 (1997) 2421.

[2] a) M.F. Hawthorne, D.C. Young, T.D. Andrews, D.V. Howe, R.L. Pilling, A.D. Pitts, M. Reintjes, L.F. Warren Jr., P.A. Wegner, J. Am. Chem. Soc. 90 (1968) 879;

b) J.N. Francis, M.F. Hawthorne, Inorg. Chem. 10 (1971) 594;

c) N.N. Greenwood, A. Earnshaw, in *Chemistry of the Elements* 2nd, Elsevier, **1997**;

d) R.N. Grimes, *Carboranes (3rd Edition).* Academic Press, US, 2016.

[3] a) J. Plesek, Chem. Rev. 92 (1992) 269.

[4] I.B. Sivaev, V.I. Bregadze, Collect. Czeck. Chem. Commun. 64 (1999) 783.

[5] a) D. Olid, R. Núñez, C. Viñas, F. Teixidor, Chem. Soc. Rev. 42 (2013) 3318;

b) S. A. Anufriev, I. B. Sivaev, V. I. Bregadze, Russ. Chem. Bull. Intl. Ed. 64 (2015) 712;

c) A. V. Safronov, Y. V. Sevryugina, S. S. Jalisatgi, R. D. Kennedy, C. L. Barnes, M. F. Hawthorne, Inorg. Chem. 51 (2012) 2629.

[6] a) M. Corsini, F. Fabrizi de Biani, P. Zanello, Coord. Chem. Rev. 250 (2006) 1351;

b) R. Nuñez, I. Romero, F. Teixidor, C. Viñas, Chem. Soc. Rev. 45 (2016) 5147;

c) R.Núñez, M.Tarrés, A. Ferrer-Ugalde, F. Fabrizi de Biani, F. Teixidor, Chem. Rev 116 (2016) 14307.

[7] F. Teixidor, C. Viñas, Pure Appl. Chem. 84 (2012) 2457.

[8] a) P.K. Hurlburt, R.L. Miller, K.D. Abney, T.M. Foreman, R.J. Butcher, S.A. Kinkhead, Inorg. Chem. 34 (1995) 5215;

b) L. Matel, F. Macasek, P. Rajec, S. Hermanek, J. Plesek, Polyhedron 1 (1982) 511;

c) P. Selucky, K. Base, J. Plesek, S. Hermanek, J. Rais, Chem. Abstr. 104 (1986) 1866379g.

[9] a) O.N. Kazheva, G.G. Alexandrov, A.V. Kravchenko, V.A. Starodub, I.A. Lobanova, I.B. Sivaev, V.I. Bregadze, L.V. Titov, L.I. Buravov, O.A. Dyachenko, J. Organomet. Chem. 694 (2009) 2336;

b) L.I. Zakharkin, V.A. Olshevskaya, E.V. Balagurova, P.V. Petrovskii, Russ. J. Gen. Chem. 70 (2000) 550;

c) O.N. Kazheva, G.G. Aleksandrov, A.V. Kravchenko, V.A. Starodub, G.G. Zhigareva, I.B. Sivaev, V.I. Bregadze, L.I. Buravov, L.V. Titov, O.A. Dyachenko, Russ. Chem. Bull. 59 (2010) 1137.

[10] P. González-Cardoso, A.I. Stoica, P. Farràs, A. Pepiol, C. Viñas, F. Teixidor, Chem. Eur. J. 16 (2010) 6660.

[11] A. Pepiol, F. Teixidor, R. Sillanpää, M. Lupu, C. Viñas, Angew. Chem. Int. Ed. 50 (2011) 12491.

[12] a) M. Tarres, E. Canetta, C. Viñas, F. Teixidor, A.J. Harwood, Chem. Commun. 50 (2014) 3370;

b) M. Tarres, E. Canetta, E. Paul, J. Forbes, K. Azzouni, C. Viñas, F. Teixidor, A.J. Harwood, Sci. Rep. 5 (2015) 7804.

[13] K.J. Winberg, G. Barberà, L. Eriksson, F. Teixidor, V. Tolmachev, C. Viñas, S. Sjöberg. J. Organomet. Chem. 680 (2003) 188.

[14] K.B. Gona, A. Zaulet, V. Gómez-Vallejo, F. Teixidor, J. Llop, C. Viñas, Chem Commun 50 (2014) 11415.

[15] a) P. Rezacova, P. Cígler, P. Matejicek, M. Lepsik, J. Pokorna, B. Gruner, J. Konvalinka, Chapter 3 p. 41 in Boron Science: New Technologies and Applications (Ed.: N. S. Hosmane), CRC Press, Boca Raton, **2012**;

b) B.P. Dash, R. Satapathy, B.R. Swain, C.S. Mahanta, B. Jena, N. S. Hosmane, J. Organomet. Chem. 849-850 (2017) 170;

c) T. Popova, A. Zaulet, F. Teixidor, R. Alexandrovac, C. Viñas, J. Organomet. Chem. 747 (2013) 229;

d) Y. Zheng, W. Liu, Y. Chen, H. Jiang, H. Yan, I. Kosenko, L. Chekulaeva, I. Sivaev, V. Bregadze, X. Wang, Organometallics 36 (2017) 3484.

[16] a) G.W. Kabalka, Chapter 5 p. 91 in Boron Science: New Technologies and Applications (Ed.: N. S. Hosmane), CRC Press, Boca Raton, **2012**;

b) H.K. Agarwal, S.Hasabelnaby, R. Tiwari, W. Tjarks, Chapter 6 p. 107 in Boron Science: New Technologies and Applications (Ed.: N. S. Hosmane), CRC Press, Boca Raton, **2012**.

17 a) P. Bauduin, S. Prevost, P. Farràs, F. Teixidor, O. Diat, T. Zemb, Angew. Chem. Int. Ed. 50 (2011) 5298;

b) P. Matějíček, P. Cígler, K. Procházka, V. Král, Langmuir 22 (2006) 575;

c) D. Brusselle, P. Bauduin, L. Girard, A. Zaulet, C. Viñas, F. Teixidor, I. Ly, O. Diat, Angew. Chem. Int. Ed. 52 (2013) 12114.

d) V. Ďordovic,˘ Z. Tosner, M. Uchman, A. Zhigunov, M. Reza, J. Ruokolainen, G. Pramanik, P. Cígler, K. Kalíkova,́ M. Gradzielski, P. Matejícek, Langmuir 32 (2016) 6713.

[18] a) C. Verdia-Baguena, A. Alcaraz, V.M. Aguilella, A.M. Cioran, S.Tachikawa, H. Nakamura, F. Teixidor, C. Viñas, Chem. Commun. 50 (2014) 6700;

b) T. I. Rokitskaya, I. D. Kosenko,. I. B. Sivaev, .Y. N. Antonenkoa, V. I. Bregadze, Phys.Chem.Chem.Phys. 19 (2017) 25122.

[19] A.I. Stoica, C. Viñas, F. Teixidor, Chem. Commun. (2009) 4988.

[20] M. Tarrés, C. Viñas, P. González-Cardoso, M. M. Hänninen, R. Sillanpää, V. Dordovic, M. Uchman, F. Teixidor, P. Matejcek ,Chem. Eur. J. 20 (2014) 6786

[21] A. Popov, T. Borisova, J. Colloid and Int. Science 236 (2001) 20.

[22] E.J. Juarez-Perez, R. Nunez, C. Viñas, R. Sillanpaa, F. Teixidor, Eur. J. Inorg. Chem. 16 (2010) 2385.

[23] a) C. Masalles, S. Borrós, C. Viñas, F. Teixidor, Adv. Mat. 12 (2000) 1199;

b) C. Masalles, J. Llop, C. Viñas, F. Teixidor, Adv. Mat. 14 (2002) 826.

[24] a) J. Plešek, Chem. Rev. 92 (1992) 269;

b) R.N. Grimes, J. Chem. Educ. 81 (2004) 658.

[25] G. Chevrot, R. Schurhammer, G. Wipff, J. Phys. Chem. B. 110 (2006) 9488.

[26] C. Viñas, M. Tarrés, P. González-Cardoso, P. Farràs, P. Bauduin, F. Teixidor, Dalton Trans. 43 (2014) 5062.

[27] R. Fernandez-Alvarez, V. Ďorďovic,ˇ M. Uchman, P. Matejícek, Langmuir, DOI: 10.1021/acs.langmuir.7b03306.

[28] P.-M. Gassin, L. Girard, G. Martin-Gassin, D. Brusselle, A. Jonchère, O. Diat, C. Viñas, F. Teixidor, P. Bauduin, Langmuir 31 (2015) 2297.

[29] a) On February 28th 2017;

b) J. Bruno, J.C. Cole, P.R. Edgington, M. Kessler, C.F. Macrae, P. McCabe, J. Pearson, R. Taylor, Acta Crystallogr. B58 (2002) 389.

[30] M.J. Hardie, C.L. Raston, Angew. Chem. Int. Ed. 39 (2000) 3835.

[31] M.J. Hardie, N. Malic, C.L. Raston, B.A. Roberts, Chem. Commun. 26 (2001) 865.

[32] M.J. Hardie, C.L. Raston, Chem. Commun. 26 (2001) 905.

[33] J. Brus, A. Zhigunov, J. Czernek, L. Kobera, M. Uchman, P. Matejicek, Macromolecules 47 (2014) 6343.

[34]https://chem.libretexts.org/Core/Inorganic_Chemistry/Descriptive_Chemistry/Periodic_Trends_of_Elemental_Properties/Periodic_Trends_in_Ionic_Radii.

[35] L.F. Lindoy. The Chemistry of Macrocyclic Ligand Complexes, Cambridge University Press, Cambridge, 1989, pp. 189.

[36] a) R.H. Crabtree, P.E. M. Siegbahn, O. Eisenstein, A.L. Rheingold, T.F. Koetzle, Acc. Chem. Res. 29 (1996) 348;

b) R. Custelcean, J.E. Jackson, Angew. Chem. Int. Ed. 38 (1999) 1661;

c) P.C. Singh, G.N. Patwari, Chem. Phys. Lett. 419 (2006) 265.

[37] a) A. Zaulet. Doctoral Thesis. Bellaterra, November 20th 2015;

b) M. Uchman, V. Dordovic, Z. Tosner, P. Matejicek, Angew. Chem. Int. Ed. 54 (2015) 14113.

[38] a) J. H. Lin, W. S. Chen, S. S. Hou, J. Phys. Chem. B 117 (2013) 12076;

b) B. V. N. P. Phani Kumar, S. U. Umayal Priyadharsini, G. K. S. Prameela, A. B. Mandal, J. Colloid Interface Sci. 360 (2011) 154.

[39] J. Plešek, K. Base, F. Mares, F. Hanousek, B. Stibr, S. Heřmánek, Collect. Czeck. Chem. Commun. 49 (1984) 2776.

[40] a) Z. Janousek, J. Plesek, S. Hermanek, K. Base, L. J. Todd,W. F. Wright, Collect. Czech. Chem. Commun. 46 (1981) 2818.

b) B(6), as well as B(6'), is the unique Boron vertex that is connected to both carbon vertexes of each icosahedral cluster in the metallacarborane.

[41] Z. Serber, L. Corsini, F. Durst, V. Dötsch, Methods in Enzymology 394 (2005) 17.

[42] I. Rojo, F. Teixidor, C. Viñas, R. Kivekäs, R. Sillanpää, Chem. Eur. J. 9 (2003) 4311.

[43] I. Rojo, F. Teixidor, R. Kivekäs, R. Sillanpää, C. Viñas, Organometallics (2003) 4642.

[44] P. Farràs, F. Teixidor, R. Kivekäs, R. Sillanpää, C. Viñas, B. Grüner, I. Cisarova, Inorg. Chem. 47 (2008) 9497.

[45] In December 14th 2017, 6 crystal structures of $[I_2$-**1**$]^-$ were detected.

[46] P. Sivý, A. Preisinger,O. Baumgartner, F. Valach, B. Koren, L. Mátel, Acta Cryst. C42 (1986) 28.

[47] C. Gatti, Z. Kristallogr. 220 (2005) 399.

[48] Gaussian 09, Revision C.01, M.J. Frisch, G.W. Trucks, H.B. Schlegel, G.E. Scuseria, M.A. Robb, J.R. Cheeseman, G. Scalmani, V. Barone, G.A. Petersson, H. Nakatsuji, X. Li, M. Caricato, A.V. Marenich, J. Bloino, B.G. Janesko, R. Gomperts, B. Mennucci, H.P. Hratchian, J.V. Ortiz,

A.F. Izmaylov, J.L. Sonnenberg, D. Williams-Young, F. Ding, F. Lipparini, F. Egidi, J. Goings, B. Peng, A. Petrone, T. Henderson, D. Ranasinghe, V.G. Zakrzewski, J. Gao, N. Rega, G. Zheng, W. Liang, M. Hada, M. Ehara, K. Toyota, R. Fukuda, J. Hasegawa, M. Ishida, T. Nakajima, Y. Honda, O. Kitao, H. Nakai, T. Vreven, K. Throssell, J.A. Montgomery, Jr., J.E. Peralta, F. Ogliaro, M.J. Bearpark, J.J. Heyd, E.N. Brothers, K.N. Kudin, V.N. Staroverov, T.A. Keith, R. Kobayashi, J. Normand, K. Raghavachari, A.P. Rendell, J.C. Burant, S.S. Iyengar, J. Tomasi, M. Cossi, J.M. Millam, M. Klene, C. Adamo, R. Cammi, J.W. Ochterski, R.L. Martin, K. Morokuma, O. Farkas, J.B. Foresman, D.J. Fox, Gaussian, Inc., Wallingford CT, 2009.

[49] J.P. Perdev, K. Burke, M. Ernzerhof, Phys. Rev. Lett. 78 (1997) 1396.

[50] D. Rappoport, F. Furche, J. Chem. Phys. 133, 2010, 134105/1.

[51] R.W.F. Bader, Atoms in Molecules: A Quantum Theory; Oxford University Press: Oxford, 1990.

[52] T.A. Keith, AIMAll (Version 12.06.03), TK Gristmill Software: Overland Park, KS, USA, 2003. http://aim. tkgristmill. com.

HIGHLIGHTS

1) Salts of H^+, Na^+, K^+ and Li^+ of cobaltabisdicarbollide anions were prepared to decipher the role of the cation in aggregates formation in water.

2) The $^{11}B\{^1H\}$-NMR is an excellent probe to visualize the phase transition between vesicles/monomer and micelles/monomer in cobaltabisdicarbollide anions.

3) The intermolecular $B\text{-}H_B^{\delta-}\cdots^{\delta+}H_C\text{-}C$ interactions have a major role in the formation of the self-assembly of the cobaltabisdicarbollide anions in aggregates.